第 35 卷第 9 期
2019 年 9 月

无 机 化 学 学 报
CHINESE JOURNAL OF INORGANIC CHEMISTRY

Vol.35 No.9
1665-1677

表面缺陷 α-Fe_2O_3(001)纳米片双活性位点类芬顿催化剂用于降解污染物

邱江源[1] 肖碧源[1] 覃方红[1] 张美婷[1] 万 婷[2] 刘锦萍[1] 陈建华*[,3] 黄在银*[,1]

([1]广西民族大学化学化工学院,南宁 530006)

([2]湖北地质局第六支队,孝感 432000)

([3]广西大学环境与资源学院,广西金属资源利用和环境保护中心,广西有色金属和特色材料加工重点实验室,南宁 530004)

摘要:纯 Fe_2O_3 表面活性位点较少具有较低的催化活性限制了其在多相芬顿催化体系中的应用。通常采用元素掺杂、贵金属负载以及与其它化合物质复合等改性措施来提升催化活性,然而这些措施存在催化剂制备复杂,制备成本高以及催化剂的精细结构难以精准控制等问题。因此,本文提出在 α-Fe_2O_3 表面引入氧空位缺陷构筑双活性位点(Fe^{2+}和氧空位)用于促进 H_2O_2 分解提高降解污染物降解效率。实验结果发现 α-Fe_2O_{3-x}-330/H_2O_2 体系具有较宽的 pH 使用范围(pH=2~10)。当 pH=4 时,罗丹明 B 的降解速率常数为 0.834 h^{-1},而且催化剂具有磁性,易回收重复使用。催化机理研究表明氧空位缺陷 α-Fe_2O_{3-x} 催化剂的氧空位和 Fe^{2+} 两种活性位点均可促进 H_2O_2 分解,而且氧空位的引入有利于污染物在催化剂表面的吸附进一步提高催化性能。

关键词:三氧化二铁;多相芬顿催化;羟基自由基;双活性位点;表面电子调控

中图分类号:O614 **文献标识码**:A **文章编号**:1001-4861(2019)09-1665-13

DOI:10.11862/CJIC.2019.199

Surface-Electronic-State-Modulated, Single-Crystalline (001) α-Fe_2O_3 Nanosheets with Dual Reaction Sites for Efficient Fenton-Like Catalysis

QIU Jiang-Yuan[1] QIN Fang-Hong[1] XIAO Bi-Yuan[1] ZHANG Mei-Ting[1]
WAN Ting[1] LIU Jin-Ping[1] CHEN Jian-Hua*[,3] HUANG Zai-Ying*[,1]

([1]*College of Chemistry and Chemical Engineering, Guangxi University for Nationalities, Nanning* 530006, *China*)

([2]*The Sixth Geological Brigade of Hubei Geological Bureau, Xiaogan, Hubei* 432000, *China*)

([3]*School of Resources, Environment and Materials, Innovation Center for Metal Resources Utilization and Environment Protection, and Guangxi Key Laboratory of Processing for Non-ferrous Metal and Featured Materials, Guangxi University, Nanning* 530004, *China*)

Abstract: Intrinsically poor reactivity restricts hematite (α-Fe_2O_3) from heterogeneous Fenton systems. Usually, metal ion doping, noble metal loading, and compounding with other compounds to enhance their catalytic activity are necessary, making them complex, expensive, and difficult to control. Here a surface-electronic-state-modulation-based concept applied to hematite is presented. This concept enables hematite with dual reaction sites as highly reactive and reusable Fenton-like catalysts for efficient catalytic oxidation of recalcitrant organics, via activation of H_2O_2 and without any extra energy input. The rhodamine B degradation rate constants for α-Fe_2O_{3-x}-330/H_2O_2 systems were 0.834 h^{-1}, when pH=4, and have a much wider pH working window (pH=2~10) than traditional Fenton systems. Meanwhile, the used catalyst can be easily recovered by magnetic separation. Oxygen vacancy and Fe(Ⅱ) on defective α-Fe_2O_{3-x} surfaces have been confirmed as the active sites for H_2O_2 activation,

收稿日期:2019-02-18。收修改稿日期:2019-06-22。

国家自然科学基金(No.21273050,21573048,21873022,51574092)资助项目。

*通信联系人。E-mail:huangzaiyin@163.com,jhchen@gxu.edu.cn,Tel:+86 7713262120,Fax:+86 7713261718

while the adjacent vacancy oxygens site adsorbs organic molecules and thus improves the Fenton-like catalytic performance. These findings may not only extend the environment applications of pure transition metal oxide but also stimulate new opportunities for the same as many other transition metal oxides by surface electronic-state modulation.

Keyworks: α-Fe_2O_3 nanosheets; heterogeneous fenton catalysis; hydroxyl radical; dual reaction sites; surface-electronic-state-modulated

0 Introduction

Fenton reaction as an efficient exhaustive oxidation process for advanced water treatment has drawn more due to the formation of non-selective hydroxyl radicals (·OH)[1-2]. However, traditional homogeneous Fenton systems (Fe^{2+}/H_2O_2) suffer severely from limited pH range, large iron sludge, and damage to the catalyst[3]. Therefore, the science and technology behind the enhanced catalytic performance of homogeneous Fenton systems, especially based on homogeneous Fenton transition metal ions, have attracted increasing attention over the past several decades[4-6]. for example, by adding various materials, or photo-, sono-, electro-assisting and using organic matter as the co-catalysts to enhance the generation of ·OH[7-9]. Unfortunately, the strict acidic condition to prevent iron precipitation and the poor stability during redox cycling still remains the main challenges for iron-based homogeneous Fenton systems[10]. On the other hand, organic co-catalysts can easily cause secondary pollution, making it very difficult to achieve complete mineralization of the organic molecule. Furthermore, maintaining stable activity of advanced oxidation processes with organic co-catalysts because of the self-degradation induced by the oxidation of the co-catalysts by ·OH is difficult[11].

To avoid the shortcomings of the traditional homogeneous Fenton reaction, heterogeneous Fenton systems, based on transitional metal or metal oxides in multiple oxidation states, are developed[12-15]. However, many pure transitional metal or metal oxides, it has rarely been considered a direct catalyst in heterogeneous Fenton systems due to its intrinsic poor reactivity. For example, it is hard for the dissociation of H_2O_2 to occur on the defect-free Fe_2O_3 surface in heterogeneous Fenton systems, while modified materials, such as TiO_2/Au/Fe_2O_3, S doped Fe_2O_3, and Fe@Fe_2O_3 composites, show high performance in the degradation of pollutants, making them complex and expensive[16-18]. Currently, like many other transition metal oxides, it is still very challenging to apply a pure Fe_2O_3-based catalyst directly for heterogeneous Fenton systems.

It has been reported that oxygen vacancy defects are able to modulate the surface-electron state and serve as active sites for redox reactions[19,20]. Furthermore, surface oxygen vacancy defects can modulate both the coordination structures and electronic states of adsorbates via the surface dangling bonds and localized electrons, influencing the kinetics, energetics, and the mechanisms of catalytic processes[21]. Recently, Mao et al. reported that oxygen vacancy concentration enhanced the selectivity in photocatalytic oxidation of amines to imines[22]. They found that BiClO surface oxygen vacancy concentration could alter the molecular oxygen activation pathway as well as the mechanisms of catalytic processes. According to Li et al., based on BiClO surface oxygen vacancy of electron-donor nature for the heterolytic H_2O_2 dissociation, generated ·OH could effectively degrade organic pollutants in the pH range of 3~10, having a much wider pH working window than traditional Fenton systems[23]. Xing et al. reported that unsaturated S atoms on the surface of metal sulfides expose metallic active sites with reductive properties, which can serve as excellent co-catalysts to greatly increase the efficiency of H_2O_2 decomposition[24]. Sun et al. using density functional theory calculations, conducted an investigation into the adsorption characteristics of H_2O_2 on defect-free and oxygen vacancy defect of α-Fe_2O_{3-x} (001) surfaces. The results show that H_2O_2

adsorption on a defect-free surface was also in a molecular form. However, on defect-containing α-Fe_2O_3 (001) surface oxygen vacancy remarkably enhanced the adsorption intensities of H_2O_2 and oxygen vacancy and Fe^{2+} as the "Fenton-catalytic" center to promote H_2O_2 decomposition on the catalyst surface[25]. Considering these oxygen vacancy and Fe^{2+} reaction sites for H_2O_2 activation and oxygen vacancy with the excellent adsorption property of vacancy oxygen α-Fe_2O_{3-x} these factors. Herein, we put a surface-electronic-state-modulation-based concept utilizing oxygen vacancy defect α-Fe_2O_{3-x} (001) surfaces with dual reaction sites for dissociation H_2O_2, thus expected to be effective in improving the Fenton-like catalysis.

We select α-Fe_2O_3, a typical transitional metal oxide with high earth abundance and low toxicity, as the model catalyst to check this possibility. In this study, we construct a surface Fenton system with defective α-Fe_2O_{3-x} (001) nanosheets, and H_2O_2 (α-Fe_2O_{3-x}(001)/H_2O_2) to degrade various organic pollutants, including *p*-nitrophenol, methylene blue, and rhodamine B. The presence of surface Fe^{2+} ion and OVs is confirmed by X-ray photoelectron spectroscopy (XPS) and Raman spectroscopy. The electron spin resonance (ESR), 1,10-phenanthroline complexant experiment proved that Fe^{2+} and oxygen vacancy on defect-containing α-Fe_2O_{3-x} surfaces as the "Fenton-catalytic" center for dissociate H_2O_2 to produce ·OH. Moreover, the stability and the reusability of defective α-Fe_2O_{3-x} (001) nanosheets are also investigated.

1 Experimental

1.1 Chemicals

$FeCl_3·6H_2O$, NaOH, HCl, H_2O_2 (30%, *w*/*w*), sodium acetate, ethyl alcohol rhodamine B (RhB), methylene blue (MB), *p*-nitrophenol (PNP), *tert*-butyl alcohol (TBA), hydroxylamine hydrochloride 1,10-phenanthroline, and sodium acetate; all of analytical grade were used as received without any further purification and bought from Medicines Corporation Macklin. Milli-Q water (18 MΩ cm in resistivity, Millipore Corporation) was used throughout the experiments. All the concentra-tions of organic pollutant solutions were 20 $mg·L^{-1}$. The aqueous NaOH (0.1 $mol·L^{-1}$) and HCl (0.1 $mol·L^{-1}$) solutions were utilized to adjust the pH values of the degradation solutions. H_2O_2 solutions were freshly prepared before use and covered with foil paper to protect them from light.

1.2 α-Fe_2O_3 nanosheets preparation

The synthesis of α-Fe_2O_3 nanosheets, was based on previous reported methods[26]. Briefly, $FeCl_3·6H_2O$ (1 g) was dissolved under vigorous stirring in ethanol (40 mL) with Milli-Q water (2.8 mL). Afterward, sodium acetate (3.2 g) was added under stirring. Then, the mixture was sealed in a Teflon-lined stainless steel autoclave and heated at 180 ℃ for 12 h. Upon cooling to room temperature, the obtained products were washed with Milli-Q water and ethanol several times, respectively, and dried at 65 ℃ for 12 h. Then, the products were annealed in H_2 atmosphere (10% H_2+90% Ar, *V*/*V*)) at different temperatures (25, 300, 350) for 2 h at a ramp rate of 10 $℃·min^{-1}$ (the samples were designated as T-1, α-Fe_2O_3-25, T-2, α-Fe_2O_3-300, T-3, and α-Fe_2O_3-330, respectively).

1.3 Characterization

Morphology and structure were characterized by high-resolution transmission electron microscopy (HR-TEM) measurements (Model No. JEM-2010, JEOL, Ltd., Tokyo, Japan). X-ray diffraction (XRD) patterns were recorded on a Philips X′Pert Pro X-ray diffractometer with Cu *K*α radiation (0.154 18 nm, *U*=40 kV, *I*=40 mV, 2θ=20°~80°). XPS data were obtained using Perkin-Elmer PHI 5000C, and all binding energies were corrected for specimen charging by referencing the C1*s* peak to 284.8 eV. Raman measurements were carried out on a Lab RAM HR800 confocal microscope Raman system (Horiba Jobin Yvon, Inc., USA). The infrared spectra were recorded between 4 000 and 600 cm^{-1} on a Fourier transform-infrared spectrometer (FT-IR) (MagnaIR 750, Nicolet Instrument, Inc., USA). The surface charge was determined by a Zetasizer Nano ZSP. The scanning electron microscope (SEM) images were obtained with a SU8010 field-emission scanning electron microscope (Hitachi, Japan).

1.4 Degradation procedures

Batch trials were carried out in 50 mL conical

flasks under shaking table concentrator at (25±2) ℃. Briefly, the reactions were triggered by adding 10 mg of catalyst (T-1, T-2, T-3) and 1 mL of 0.5 mol·L^{-1} H_2O_2 solution into 20 mL of rhodamine B solution (20 mg·L^{-1}) in sequence. After that, 800 μL of the reaction solution was sampled at predetermined intervals. Followed by high-speed centrifugation and collection of the supernatant solution for the rhodamine B concentration measurement, 0.1 mol·L^{-1} HCl and 0.1 mol·L^{-1} NaOH were used to adjust the initial pH values of the reaction solutions. To assess the stability of T-3, the catalyst after reaction was separated from the solution, then washed thoroughly with deionized water and ethanol, and finally vacuum-dried for the reuse. Besides rhodamine B, degradation experiments on other organic pollutants, including methylene blue and *p*-nitrophenol were also conducted. All the other experimental procedures were the same as those of rhodamine B degradation.

1.5 Analytical methods

The solution (methylene blue, rhodamine B, *p*-nitrophenol) was directly added to a 1 cm×1 cm glass cell before being measured at a variable wavelength mode, using a UV-Vis spectrophotometer (Phenix Optical Co. Ltd). The absorbance at 660, 554, and 317 nm, respectively, was used for the quantification. The pollutant removal efficiency was obtained by using the equation (**1**):

$$\eta=\frac{C_0-C}{C_0} \quad (1)$$

η is the removal efficiency (%), C_0, and C are the initial concentrations and moment concentration at time t of pollutants, respectively. The concentrations of dissolved iron ions were detected with inductively coupled plasma optical emission spectrometer (ICP-OES, Agilent, Varian 700) in some cases. The ·OH radicals were detected via ESR using 5,5-dimethyl-1-pyrroline-*N*-oxide as the radical spin-trapped reagent (Bruker A200, Germany).

2 Results and discussion

2.1 Morphology and structure of Fe_2O_3 nanosheets

The structure and oxidation state of the as-prepared α-Fe_2O_3 architectures were characterized using XRD, Raman spectra, infrared spectrum, and high-resolution XPS. The morphology and crystallinity of as-prepared α-Fe_2O_3 architectures were analyzed using SEM, high-resolution HR-TEM. T-1 (Fig.1a), T-2

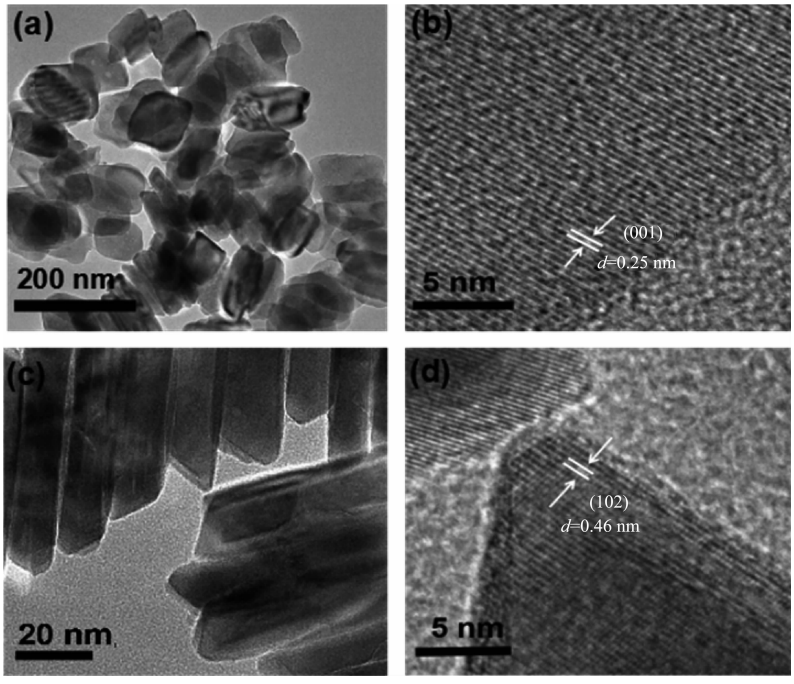

(a) Overview TEM images; (c) Thickness TEM images of α-Fe_2O_{3-x}; (b) and (d) The (001) and (102) facets are marked

Fig.1 Morphology and structure of the α-Fe_2O_{3-x} nanosheets

(Fig.2a), and T-3 (Fig.2b) exhibit a similar morphology. Based on SEM and TEM analysis (Fig.S1), the width and thickness of the plates is determined to be 161.17 nm and 27.93 nm, respectively. A representative HR-TEM image shows the (001) crystal facet with a lattice fringe of 0.25 nm in Fig.1(b). The (102) crystal facet, in the lower part, shows a lattice spacing of 0.46 nm Fig.1(d) suggesting that the bottom/top surfaces are enclosed by the (001) facet[26]. As shown in Fig.2(c) and (d), disordered lattice fringes induced by defects for T-2 and T-3 are shown. Moreover, T-1, T-2, and T-3 exhibit a similar morphology, indicating that the high-temperature conditions do not cause further changes in the morphology. The XRD patterns in Fig. 3(a) show that the as-prepared T-1, T-2, and T-3 are monoclinic phase, and the diffraction peaks match well with T-1, T-2 (Hematite, PDF No.33-0664). However, T-3 generates a new peak at 30.04° which matches with Fe_3O_4 (PDF No.19-0629), and a peak disappears at 24.8°, with the results showing that the crystal structure has changed[27]. However, from XRD it is hard to discriminate that the reduction of α-Fe_2O_3 may produce some Fe_3O_4 on the surface. Therefore, Raman spectra and infrared spectrum were recorded for these samples. However, in Fig.3(c), the Raman spectra of the T-3 contain strong peaks at around 224 (A_g), 287 (E_g), and 402 cm^{-1} (E_g), indicating that are mainly composed of hematite α-Fe_2O_3 [28], and no peaks referring to Fe_3O_4 are found at 665 cm^{-1} [29]. Furthermore, in the infrared spectrum (Fig.3(b)), there are no peaks referr-ing to Fe_3O_4 found at 568 cm^{-1} on the T-3 surface[30]. This result shows that T-3 is comprised of an intermed-iate state of α-Fe_2O_3 to Fe_3O_4 and excludes the formation of Fe_3O_4 on the T-3 surface, which leads it to show the magnetic properties of the T-3 catalyst[31-32].

However, on the T-3 surface, there is no formation of Fe_3O_4, as verified by Raman spectra and infrared spectrum analysis. It is noted that the red-brown Fe_2O_3 changes to brown-black (Fig.S2(a)), indicating that the surface of Fe_2O_3 particles is partly reduced during the reaction. The Fe oxidation state was probed by XPS, and Raman spectra, respectively. The surface iron species were investigated by XPS analysis, using the $Fe2p_{3/2}$ spectral region. After the hydrogen treatment, the T-2 and T-3 samples, an evident shoulder appeared in the negative shift of the $Fe2p_{3/2}$ spectrum (Fig.3(d)), which suggests that Fe(Ⅱ) was generated on the α-Fe_2O_3 surface[33]. This clearly shows that the surface of Fe_2O_3 is partly reduced in the hydrogenation reaction. Peak positions are shifted toward lower wave numbers and their full width at

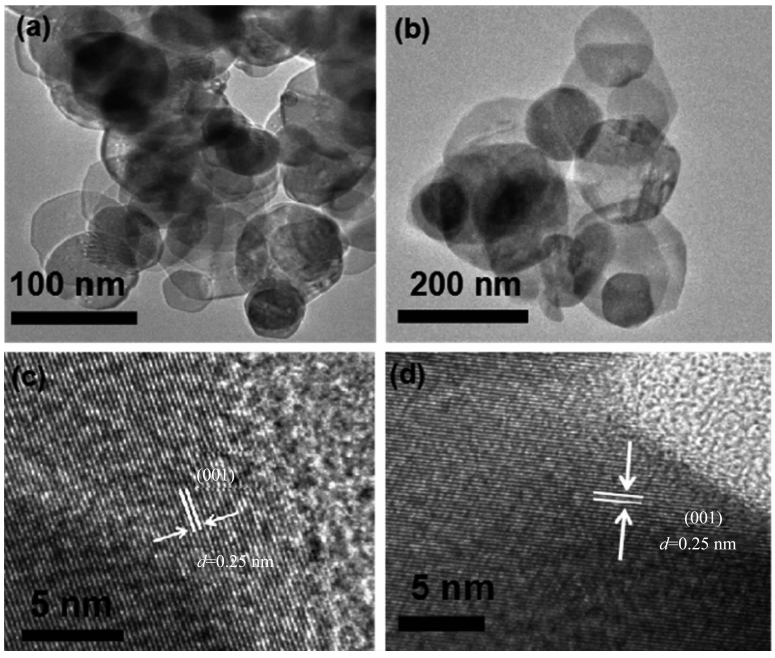

Fig.2　(a) and (b) Overview TEM images of T-2, T-3; (c) and (d) Disordered lattice structures of T-2 and T-3 are highlighted

half-maximum values are increased in the Raman spectra from T-2 and T-3, compared with those of T-1 (Fig.3(e)). These results suggest that more oxygen vacancies T-2, T-3 are introduced into oxygen-deficient α-Fe_2O_{3-x}[34]. To describe the presence of oxygen vacancies qualitatively in the oxygen-deficient T-2 and T-3 surfaces, the UV-Vis absorption spectra are acquired. As shown in Fig.3(f), the wavelength absorption ranges of the T-2 and T-3 gradually shift more toward the visible light region. Such phenomena can be attributed to the increased oxygen vacancies on the T-2 and T-3 surfaces[35]. Therefore, based on the results of these Raman, XPS analyses, UV-Vis absorption spectra, and FT-IR spectrum, we demonstrate that oxygen vacancies and Fe^{2+} are created in both T-2 and T-3 surfaces.

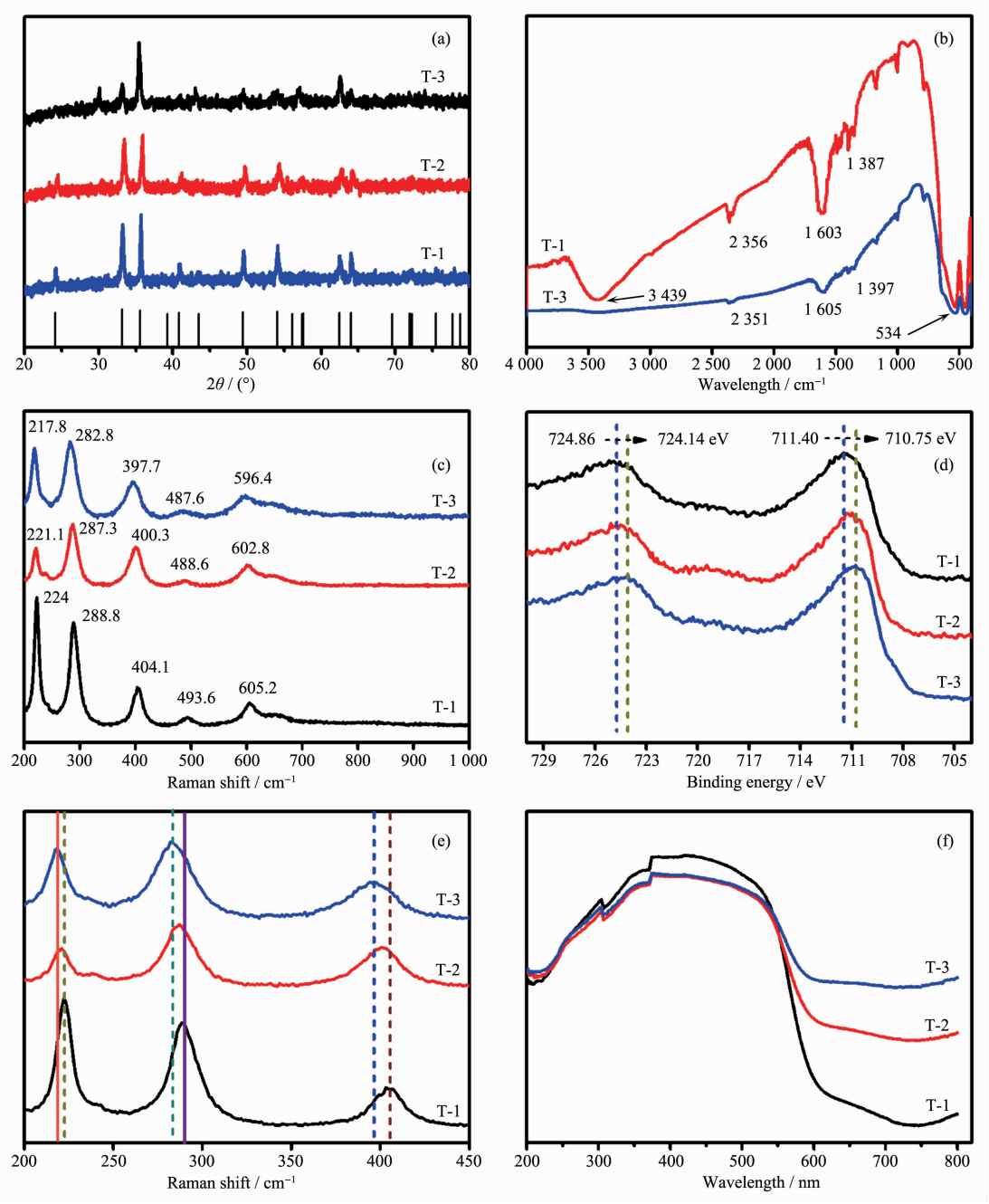

(a) XRD patterns; (b) FT-IR spectra; (c) Raman spectra; (d) XPS of the α-Fe_2O_{3-x} nanosheets; (e) Raman spectra; (f) Solid ultraviolet visible spectrum of the α-Fe_2O_{3-x} nanosheets

Fig.3 Structure and surface-electronic-state characterizations

2.2 Catalytic activity

The catalytic activity of the as-prepared catalyst was evaluated by degrading rhodamine B model pollutants. As shown in Fig.4 (a), in the presence of H_2O_2, about 78.8% and 91.6% of rhodamine B was degraded in the T-2 and T-3 systems within 4 h, respectively. However, rhodamine B removal efficiency was only 9.1% over T-1 /H_2O_2 systems under the same conditions, much lower than that (>78%) in the T-2 and T-3 systems with pH=7. To give a clear comparison of the catalytic performance, the RhB removal kinetics was fitted by the first-order reaction (Fig.S3(a)). As shown in Fig.4(b), the reaction constants for T-1/H_2O_2 systems, T-2/H_2O_2 systems, and T-3/H_2O_2 systems were 0.019 3, 0.425, and 0.534 h^{-1}, respectively. The reaction rate constant (K_a) values for the T-2 and T-3 systems were 22.02 and 27.66 times that of the T-1 systems, respectively. Since the T-1, T-2, and T-3 surfaces exhibit similar morphology and phase, the discrepancies in the catalytic activity can be ascribed to the surface defects.

Since heterogeneous Fenton process are always considered to be complex systems and many factors can affect their performance, we used the T-3 systems as a model reaction and investigated a number of factors that may have an influence on heterogeneous Fenton process performance, such as the pH value, H_2O_2, and T-3 catalyst dosage. The pH of the bulk solution is known to play a governing role in the Fenton and Fenton-like systems. Many of the transitional metal heterogeneous Fenton catalysts were restricted to acidic conditions, and a significant decrease in catalytic activity was observed in neutral or even alkaline condition. However, in this study, as shown in Fig.4 (c), T-3/H_2O_2 systems always exhibited an efficient catalytic activity over a wide pH range from 2 to 10, and rhodamine B was degraded by 77.3% ~100%, and the rate constants were 0.363 4~1.007 6

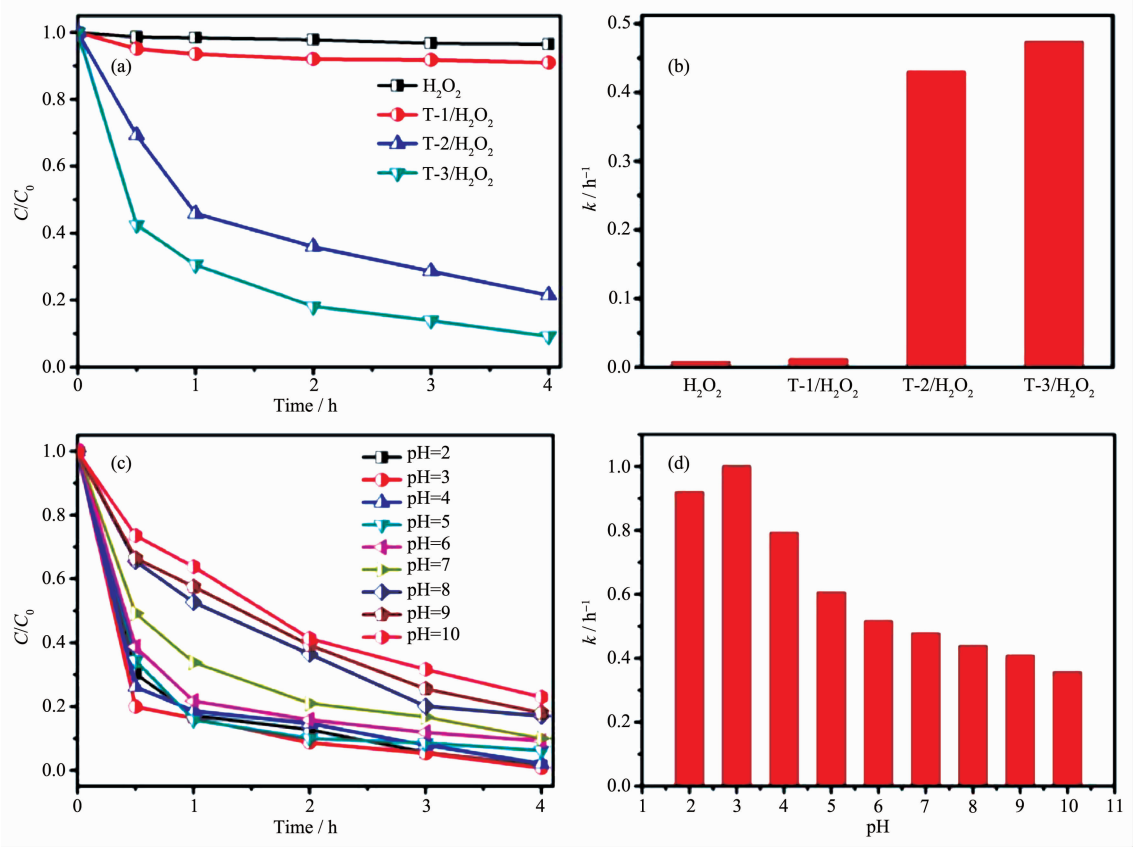

Initial RHB and H_2O_2 concentration were 20 mg·L^{-1}, 50 mmol·L^{-1}; the dosage of T-3 was 0.5 g·L^{-1}; the initial pH was 7.0

Fig.4 (a, b) Time profiles of the RhB remove efficiency and kinetic rate constant in different systems; (c) and (d) Time profiles of RhB degradation and kinetic rate constant in the T-3/H_2O_2 system at different pH conditions

h^{-1} (Fig.4(d)), validating its efficient application for real wastewater. We then monitored the surface charge of T-3 via zeta potential measurement and found that surface of T-3 was negatively charged, with the pH increase as the surface negative charge decreased (Fig.S3 (a)). The latter observation might be linked to the pH increase and the gradual increase of OH^- concentration. OH^- were supposed to be preferen-tially adsorbed on surface Fe atoms of T-3 that might compete with the RhB adsorption of T-3 (Fig.S3(b)). Therefore, the decreased adsorption of RhB over T-3 accounted for its lower reactivity under higher pH. Furthermore, as shown in Fig.S3(b) and Fig.4(d), the RhB adsorption efficiency was found to be correlated well to the Fenton-like performance, and a higher adsorption efficiency would always lead to a higher value of k in the RhB removal. Since 0.1 mol·L^{-1} HCl and 0.1 mol·L^{-1} NaOH were used for the adjustment of the system pH in the experiments, the influence of NaCl on the catalytic performance of T-3/H_2O_2 system was studied. The results in Fig.S1 (b) showed that NaCl had no obvious influence on the catalytic activity. As shown in Fig.5 (a), the H_2O_2 dosage was the important factor in rhodamine B degradation efficiency. It can be seen that only 35.2% of rhodamine B was removed with the H_2O_2 concentration lower than 2.5 mmol·L^{-1}, but its removal efficiency increases dramatically from 0 to 90.4% with a concentration ranging from 2.5 mmol·L^{-1} to 100 mmol·L^{-1}. Furthermore, appropriate increasing of the dosage of H_2O_2 can improve reaction rates of advanced oxidation processes.

To highlight the potential of defects in α-Fe_2O_3 heterogeneous catalysts for advanced water treatment for industrial applications, the catalytic stability of the constructed T-3/H_2O_2 systems was estimated by recycling the used T-3 for cyclic rhodamine B degradation in the presence of H_2O_2 as a common

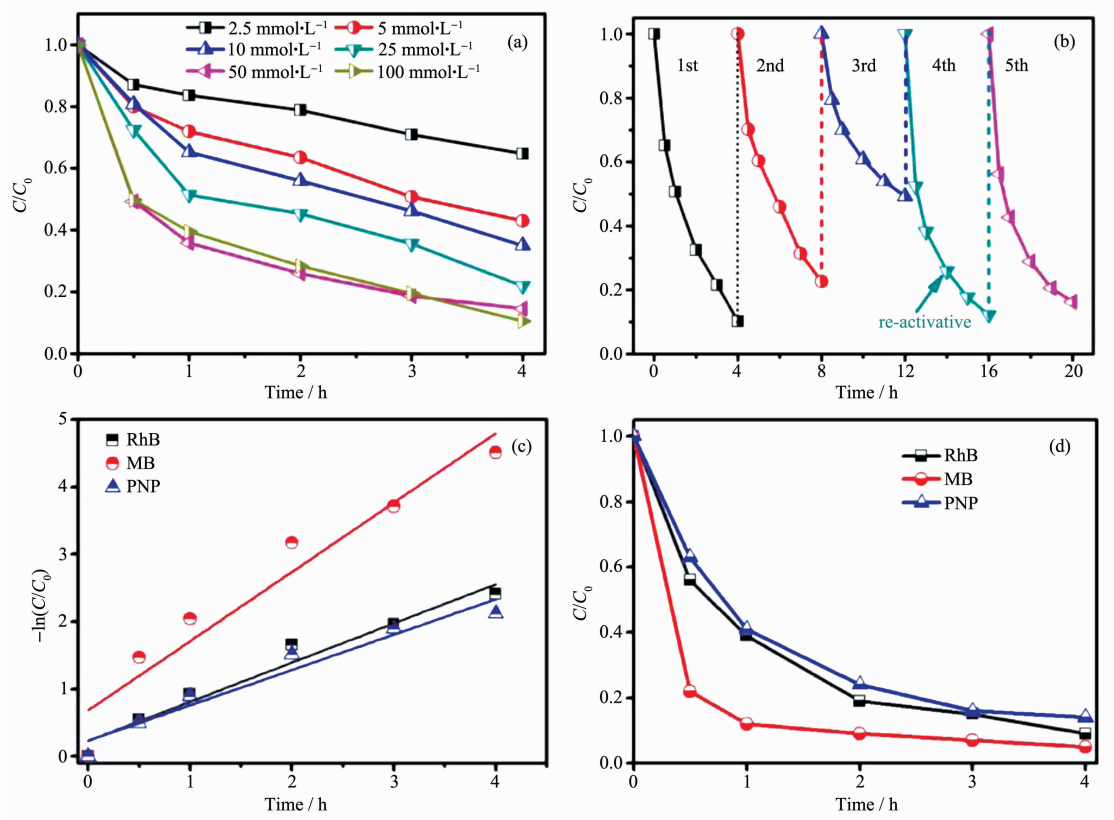

Initial RhB and H_2O_2 concentration were 20 mg·L^{-1}, 50 mmol·L^{-1}; the dosage of T-3 was 0.5 g·L^{-1}; the initial pH value was 7.0

Fig.5 (a) Time profiles of RhB degradation and kinetic rate constant in the T-3/H_2O_2 system at different initial H_2O_2 concentration, (b) Reusability of T-3 for the degradation of RhB in the T-3/H_2O_2 system, (c) and (d) PNP/MB/RhB degradation kinetic rate constant and remove efficiency in T-3/H_2O_2 systems

oxidant. It can be seen from Fig.5(b) that when pH is 7, after recycling three times, the recycled oxidative removal of RhB T-3/H_2O_2 systems gradually loses about 44% of their initial reactivity. After the reactivation of T-3 via the same thermal treatment, however, reusability of catalyst for organic pollutants oxidation is suggested at pH=7. The after-reactivation of T-3 was further validated by Raman, XRD, SEM analysis. As shown in Fig.S4, the morphology and structure of the T-3 catalyst had no obvious change after recycling five times, indicating its good stability. Furthermore, as shown in Fig.S5, the used catalyst can be easily recovered by magnetic separation. Moreover, rhodamine B (20 mg·L^{-1}), methylene blue (20 mg·L^{-1}), and *p*-nitrophenol (20 mg·L^{-1}) can be efficiently degraded (reaction rate constant K_a values of rhodamine B (20 mg·L^{-1}); methylene blue (20 mg·L^{-1}) and *p*-nitrophenol (20 mg·L^{-1}) were 0.575, 0.895 and 0.515 h^{-1}, respectively (Fig.5(c) and (d)). Subsequently, we scaled up our testing system from 20 mL to 1.5 L (Fig. S6(a)). As shown in Fig.S6(b), the T-3 systems still displayed excellent catalytic performance, further suggesting the potential of defect-containing α-Fe_2O_{3-x} heterogeneous catalyst in advanced water treatment for industrial applications.

We observed another interesting phenomenon. Oxygen vacancy remarkably enhanced the adsorption intensities of RhB on the catalyst surfaces. As shown in Fig.6(a) and (b), a much faster adsorption equilibrium of within 10 min, with RhB adsorption efficiency as high as 26.4%, could be achieved on T-3. This result may like ultrathin vacancy oxygen BiOCl nanosheets defects with negative charges which favors the adsorption of positively charged RhB molecules[36]. The RhB adsorption efficiency was found to be correlated well to the Fenton-like performance, and a higher adsorption efficiency would always lead to a higher value of *k* in RhB removal. These results suggest that the excellent Fenton-like performance of T-3 may result from the balanced adsorption of RhB and activation of H_2O_2.

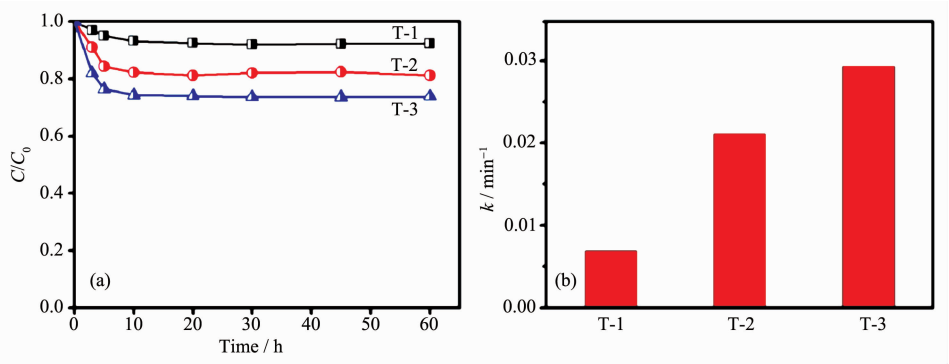

Reaction condition: c_{RhB}=20 mg·L^{-1}, $c_{catalyst}$=0.5 g·L^{-1}, and initial solution pH=7.0

Fig.6 (a) RhB adsorption efficiency of different catalysts; (b) Rate constant catalysts of different catalytic systems

2.3 Possible catalytic mechanism

Sun first used the density functional theory calculations were conducted by investigating the adsorption and reaction characteristics of H_2O_2 on perfect and oxygen defect α-Fe_2O_{3-x} (001) surfaces[25]. The results indicate that, on the defect-free α-Fe_2O_3 (001) surfaces, the H_2O_2 was parallel to the α-Fe_2O_{3-x} (001) surface and bonded with an Fe atom of the surface. The bond length of Fe-O reached 0.214 4 nm. Hydrogen bonds were also formed between two H atoms of H_2O_2 and two surface oxygen atoms with representative bond lengths of 0.147 4 and 0.148 0 nm, which are slightly longer than the calculated value for the free H_2O_2 (0.147 4 nm). According to the adsorption energy and the representative lengths of O-O and Fe-O, dissociation of H_2O_2 did not occur on the defect-free α-Fe_2O_3 (001) surface. However, on the oxygen defect α-Fe_2O_{3-x} (001) surface, the best stable chemisorption is the H_2O_2 molecule presumably dissociates into two surface hydroxyls and adsorption energy of reached to −456.66 kJ·mol^{-1}. One of the hydroxyls occupied the oxygen vacancy site ((001)-

OV +H_2O_2 →(001)-OH^-+·OH) and bonded with two surface Fe atoms (≡Fe(Ⅱ)+H_2O_2→≡Fe(III)-OH+·OH) with bond lengths of 0.205 0 and 0.203 0 nm, which donated a short of ·OH (0.186 nm) to nearby hydroxyl groups, indicating its radical nature[25,37]. Analyses of Mulliken population, electron density difference, and partial density of states showed that H_2O_2 decomposition on the oxygen defect α-Fe_2O_{3-x} (001) surface followed the Haber-Weiss mechanism, in which the electron transfers from the surface Fe atom to H_2O_2 molecule and creates hydroxyl radicals[38-39].

The above report suggests that Fe atoms close to the oxygen vacancy and localized electron donation from oxygen vacancy have stronger reducibility to adsorbed H_2O_2 could directly facilitate the H_2O_2 dissociation in a Fenton reaction manner[25]. Subsequently, we monitored the change of the chemical environment of oxygen element by X-ray photoelectron spectroscopy (XPS) analysis on the oxygen defect α-Fe_2O_{3-x} (001) surface before and after the H_2O_2 dissociation. As depicted in Fig.7(a) and (b), the O1*s* spectrum of oxygen defect α-Fe_2O_{3-x} (001) could be divided into four peaks. The O1*s* peaks at 529.7 and 530.5 eV were attributed to the lattice oxygen (Fe-O) and lattice oxygen (O^{2-}) of oxygen defect α-Fe_2O_{3-x} (001), respectively[39-40]. The binding energy of 531.7 eV which was ascribed to the -O_2^{2-} groups was adsorbed on α-Fe_2O_{3-x} surfaces and 533.2 eV for α-Fe_2O_{3-x} are assigned to hydroxyl groups (Fe-OH adsorbed) and water present on the α-Fe_2O_{3-x} as a result of the adsorption and dissociation of water[40-42]. As expected, We found at 533.3 eV increased obviously for oxygen defect α-Fe_2O_{3-x} in the α-Fe_2O_{3-x} (001)/H_2O_2 system (Fig.7b). These phenomena similar to the generation of surfacebound ·OH via the H_2O_2 decomposition in α-FeOOH-HA/H_2O_2 and BOCl-010-OV/H_2O_2[23,43].

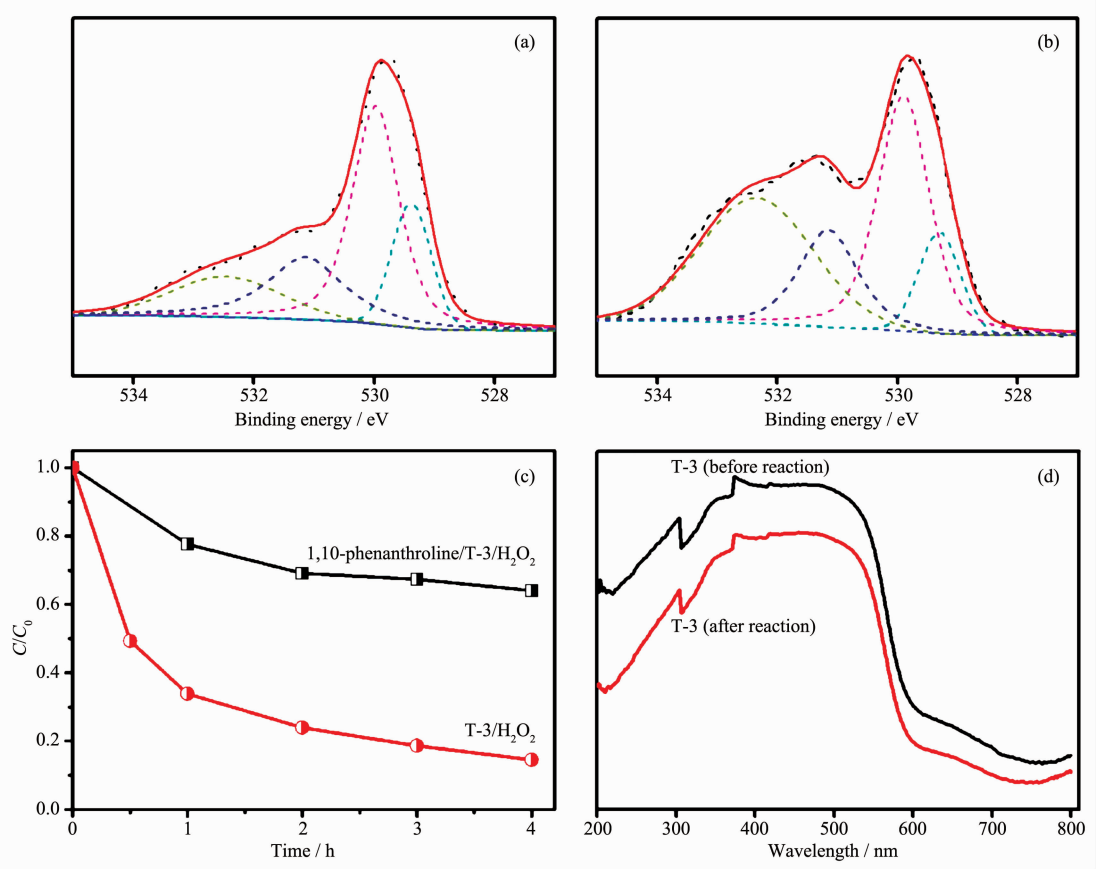

Initial RhB, H_2O_2, 1,10-phenanthroline concentration were 20 mg·L^{-1}, 50 mmol·L^{-1}, 0.01 mol·L^{-1}; the dosage of T-3 was 0.5 g·L^{-1}; the initial pH value was 7.0

Fig.7 (a) O1*s* XPS spectra of the T-3; (b) O1*s* XPS spectra of the T-3/H_2O_2; (c) 1,10-phenanthroline as the Fe^{2+} complexant; (d) Solid ultraviolet visible spectrum of T-3 before and after the RhB degradation

In this study, radical quenching experiments were conducted to identify the active radical species generated during H_2O_2 activation. As shown in Fig.8 (a), if TBA, a radical scavenger for ·OH, was added to the T-3/H_2O_2 system, the RhB degradation efficiency decreased slightly, suggesting that ·OH was the major reactive species in the T-3/H_2O_2 system. To test these theoretical results in the Fenton-like reaction, N-oxide (DMPO) was used as a spin trap in electron paramagnetic resonance (EPR) tests to detect the spin reactive ·OH adsorbed on α-Fe_2O_3 (001) surfaces or dissolved in water. No obvious EPR signal was observed over α-Fe_2O_3 (001) in the presence of H_2O_2, confirming that defect-free α-Fe_2O_3 (001) surfaces were not able to dissociate H_2O_2 for ·OH generation. As expected, strong four-line EPR spectra, with relative intensities of 1:2:2:1 corresponding to DMPO-·OH adduct were observed in defect-containing α-Fe_2O_3 (001) reacting with H_2O_2. Based on the Haber-Weiss mechanism, H_2O_2 decomposition induced by dissolved metal ions could be ruled out by non-leaching of Fe ions into the solution. We subsequently investigated the T-3 reduction process in the presence of H_2O_2 by ICP-OES (Fig.8b). The results show that no Fe ions were released from T-3 in the H_2O_2 solution. Therefore, we concluded that the H_2O_2 decomposition should mainly occur on the α-Fe_2O_3 (001) surfaces, as the theoretical calculations predicted. To further confirm the existence of surface bound ·OH generated on T-3, we compared the amounts of ·OH generated in the supernatants of the T-3/H_2O_2 and T-3/H_2O_2/F^- systems, with a DMPO trapped ESR technique (Fig. 8d), taking into consideration that F^- in the solution could desorb ·OH bound on defect-containing α-Fe_2O_3 surfaces by forming strong hydrogen bonds (surface bound ·OH⋯F–Fe_2O_{3-x})[44]. As expected, the addition

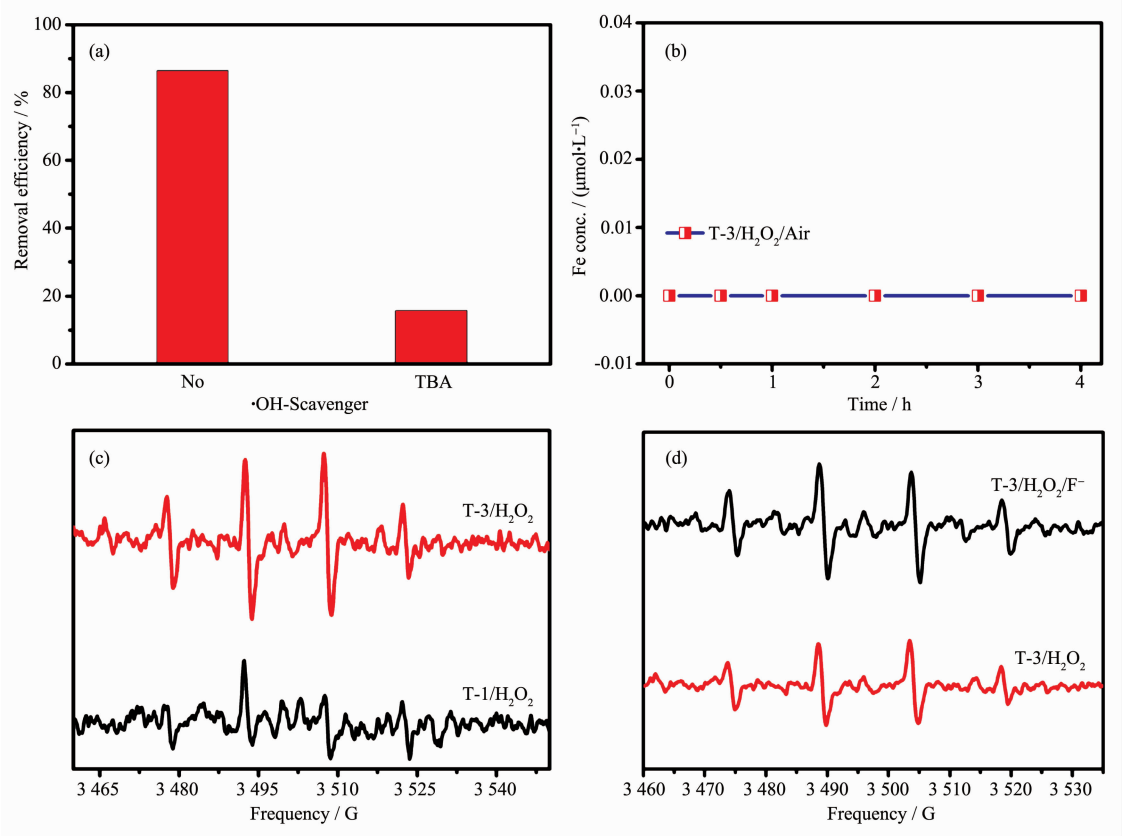

Initial RhB, H_2O_2, NaF, and TBA concentration were 20 mg·L^{-1}, 50, 2, 0.74 mmol·L^{-1}; the dosage of T-3 was 0.5 g·L^{-1}; the initial pH value was 7.0

Fig.8　(a) Degradation of RhB in the absence and presence of tert-butyl alcohol (TBA) as the ·OH scavenger, (b) DMPO trapped ESR spectra in the T-1/H_2O_2, T-3/H_2O_2 systems, (c) Changes of the total dissolved Fe concentration released from α-Fe_2O_{3-x} in the T-3/H_2O_2 systems at pH 7.0, (d) DMPO trapped ESR spectra in the T-3/H_2O_2/F^- systems

of F^- improved the intensity of the DMPO trapped ·OH ESR signal by 26.8% in the T-3/H_2O_2 system after 120 s of reaction, fully validating that the surface bound ·OH was generated by the surface on T-3 in the T-3/H_2O_2 system.

Previous studies have suggested that the oxygen vacancies and Fe^{2+} were like "catalytic active centers" promoting the decomposed H_2O_2 to produce hydroxyl and hydroxyl radical on the defect-containing α-Fe_2O_3 (001) catalyst surface[25]. To identify the chemical states of ·OH generated on the T-3 surfaces, we checked the contribution of surface Fe(Ⅱ), bound on T-3 to the rhodamine B degradation, by chelating the surface Fe (II) with 1,10-phenanthroline during the rhodamine B degradation. Interestingly, the surface Fe(Ⅱ) chelation with 1,10-phenanthroline significantly inhibited the rhodamine B degradation in the T-3/H_2O_2 system, confirming the important role of surface Fe(Ⅱ) in the rhodamine B removal within the T-3/H_2O_2 systems. However, as shown in Fig.7(c), the degradation of rhodamine B was not completely inhibited. The results suggest that the oxygen vacancy was involved in the H_2O_2 decomposition. In previous studies, it had been suggested that the oxygen vacancy concentration will be decreased in the H_2O_2 reactivation[23]. Therefore, we use UV-Vis absorption spectra to qualitatively describe the presence of defects concentration in T-3 before and after reaction. As shown in Fig.7(d), according to the absorptive capacity change of UV-Vis absorption spectra signal of T-3 (before and after), a distinct quenching of defect concentration is suggested, as the Sun theoretical calculations predicted[25]. This is attributed to the hydroxyls occupying the oxygen vacancy active site on defective α-Fe_2O_{3-x} surfaces for H_2O_2 activation and leading to defective α-Fe_2O_{3-x} surfaces oxygen vacancy concentration decrease, which is similar to oxygen vacancies in previous reports on defect-containing BiOCl systems.

3 Conclusions

In summary, we present a surface-electronic-state-modulation-based concept on pure metal oxides (α-Fe_2O_3 (001) nanocrystal) for efficient degradation of persistent organic compounds in the presence of H_2O_2. The oxygen-deficient α-Fe_2O_{3-x} catalysts prepared in this work, The dual reaction-site mechanism as displayed in Fig.9 shows, oxygen-deficient α-Fe_2O_{3-x} catalysts not only provided dual reaction sites (Fe^{2+} and oxygen vacancy) for H_2O_2 activation promoting H_2O_2 to decompose the in situ-generated ·OH. but also afforded rich oxygen vacancy sites for organic pollutant adsorption and the generated ·OH to rapid react with adjacent adsorbed pollutant, thus showing excellent Fenton-like catalytic performance. Our findings show that the surface electronic-state modulation could obviate the need for modification of many transition metal oxides with other materials, addressing poor reactivity issues.

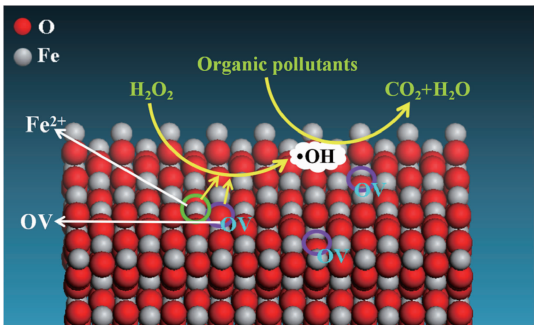

Fig.9 Proposed Fenton-like reaction mechanism on oxygen-deficient α-Fe_2O_{3-x} catalyst

Acknowledgements: The authors are thankful for the financial support from the National Natural Science Foundation of China (Grants No.21273050, 21573048, 21873022, 51574092).

Notes: No conflict of interest exits in the submission of this manuscript, and the manuscript is approved by all authors for publication. I would like to declare on behalf of my co-authors that the work described was original research and has not been under consideration for publication elsewhere, in whole or in part. All the authors listed have approved the manuscript that is enclosed.

Supporting information is available at http://www.wjhxxb.cn

References:

[1] Shannon M A, Bohn P W, Elimelech M, et al. *Nature*, **2008**, **452**(7185):301-310

[2] Garrido-Ramírez E G, Theng B K G, Mora M L. *Appl. Clay*

Sci., **2010**,**47**(3):182-192

[3] De Laat J, Le T G. *Appl. Catal. B*, **2006**,**66**(1/2):137-146

[4] Masarwa M, Cohen H, Meyerstein D, et al. *J. Am. Chem. Soc.*, **1988**,**110**(13):4293-4297

[5] Neyens E, Baeyens J. *J. Hazard. Mater.*, **2003**,**98**(1/2/3):33-50

[6] Haber F, Weiss J. *Proc. R. Soc. London Ser. A*, **1934**,**147**(861):332-351

[7] Bossmann S H, Oliveros E, Göb S, et al. *Water Sci. Technol.*, **2001**,**44**(5):257-262

[8] Bo J, Zheng J, Xiu L, et al. *Chem. Eng. J.*, **2013**,**215-216**(3):969-978

[9] Qin Y, Song F, Ai Z, et al. *Environ. Sci. Technol.*, **2015**,**49**(13):7948-7956

[10]Li T, Zhao Z, Wang Q, et al. *Water Res.*, **2016**,**105**:479-486

[11]Jiang C, Garg S, Waite T D. *Environ. Sci. Technol.*, **2015**,**49**(24):-

[12]Wang Y, Zhao H, Li M, et al. *Appl. Catal. B*, **2014**,**147**:534-545

[13]Morris R V, Lauer H V, Lawson C A, et al. *J. Geophys. Res*: *Solid Earth*, **1985**,**90**(B4):3126-3144

[14]Hosseini S G, Ahmadi R, Ghavi A, et al. *Powder Technol.*, **2015**,**278**:316-322

[15]Yang X, Xu X, Xu J, et al. *J. Am. Chem. Soc.*, **2013**,**135**(43):16058-16061

[16]Mahadik M A, Shinde S S, Pathan H M, et al. *J. Photochem. Photobiol. B*, **2014**,**141**:315-324

[17]Guo L, Chen F, Fan X, et al. *Appl. Catal. B*, **2010**,**96**(1/2):162-168

[18]Ai Z, Lu L, Li J, et al. *J. Phys. Chem. C*, **2007**,**111**(11):4087-4093

[19]Hendriksen B L M, Ackermann M D, Van Rijn R, et al. *Nat. Chem.*, **2010**,**2**(9):730

[20]Martinez U, Hansen J Ø, Lira E, et al. *Phys. Rev. Lett.*, **2012**,**109**(15):155501

[21]Li H, Li J, Ai Z, et al. *Angew. Chem., Int. Ed*, **2018**,**57**(1):122-138

[22]Mao C, Cheng H, Tian H, et al. *Appl. Catal. B*, **2018**,**228**:87-96

[23]Li H, Shang J, Yang Z, et al. *Environ. Sci. Technol*, **2017**,**51**(10):5685-5694

[24]Xing M, Xu W, Dong C, et al. *Chemistry*, **2018**,**6**(4):1359-1372

[25]Song Z, Wang B, Yu J, et al. *Appl. Surf. Sci.*, **2017**,**413**:292-301

[26]Zhou X, Lan J, Liu G, et al. *Angew. Chem. Int. Ed.*, **2012**,**51**(1):178-182

[27]Niu H, Lu J, Song J J, et al. *Ind. Eng. Chem. Res.*, **2016**,**55**(31):8527-8533

[28]De Faria D L A, Lopes F N. *Vib. Spectrosc.*, **2007**,**45**(2):117-121

[29]Xu J S, Zhu Y J. *ACS Appl. Mater. Interfaces*, **2012**,**4**(9):4752

[30]Nasrazadani S, Raman A. *Corros. Sci.*, **1993**,**34** (8):1355-1365

[31]Xu X N, Wolfus Y, Shaulov A, et al. *J. Appl. Phys.*, **2002**,**91**(7):4611-4616

[32]Wu J, Mao S, Ye Z G, et al. *ACS Appl. Mater. Interfaces*, **2010**,**2**(6):1561-1564

[33]Cao W, Tan O K, Pan J S, et al. *Mater. Chem. Phys.*, **2002**,**75**(1):67-70

[34]Liao A Z, Chen J B, Wang C W, et al. *J. Vac. Sci. Technol., B*, **2016**,**34**(2):1-8

[35]Wang J, Wang C W, Li Y, et al. *Thin Solid Films*, **2008**,**516**(21):7689-7694

[36]Guan M, Xiao C, Zhang J, et al. *J. Am. Chem. Soc.*, **2013**,**135**(28):10411-10417

[37]Chen J, Li Y F, Sit P, et al. *J. Am. Chem. Soc.*, **2013**,**135**:18774-18777

[38]Gonzalez-Olmos R, Holzer F, Kopinke F D, et al. *Appl. Catal. A*: *General.*, **2011**,**398**:44-53

[39]Dixon W T, Norman R O C. *Nature*, **1962**,**196**:891-892

[40]Baltrusaitis J, Cwiertny D M, Grassian V H. *Phys. Chem. Chem. Phys.*, **2007**,**9**:5542-5554

[41]Grosvenor A P, Kobe B A, Mcintyre N S. *Surf. Sci.*, **2004**,**572**(2):217-227

[42]Huang X, Hou X, Jia F, et al. *ACS Appl. Mater. Interfaces*, **2017**,**9**(10):8751-8758

[43]Hou X, Huang X, Jia F, et al. *Environ. Sci. Technol*, **2017**,**51**(9):5118-5126

[44]Xu Y, Lv K, Xiong Z, et al. *J. Phys. Chem. C*, **2007**,**111**(51):19024-19032